



Politecnico di Milano
Orbital Mechanics Course (A.Y. 2018/19)

FINAL ASSIGNMENTS
*Interplanetary Trajectories
& Orbit Perturbations*

Group ID: 5

Antonio Finozzi (921343)
antonio.finozzi@mail.polimi.it

Marta Padoan (915570)
marta.padoan@mail.polimi.it

Maria Francesca Palermo (920959)
mariafrancesca.palermo@mail.polimi.it

Massimo Piazza (919920)
massimo.piazza@mail.polimi.it

Contents

1 Interplanetary Explorer Mission	1
1.1 Design Process	1
1.1.1 Design Constraints	1
1.1.2 Grid Search Setup	2
1.1.3 Genetic Algorithm Setup	3
1.1.4 Selection of a Final Solution	4
1.2 Results and Conclusions	5
1.2.1 Heliocentric Trajectories	5
1.2.2 Powered Gravity Assist	7
1.2.3 Total Mission Cost	8
2 Planetary Explorer Mission	9
2.1 Initial Orbit Characterization	9
2.2 Ground Track	10
2.2.1 Ground Track Repetition	11
2.3 Orbit Propagation	12
2.4 Spectral Frequency Analysis	15
2.5 Comparison with Real Data	17

Nomenclature & Acronyms

Nondimensional Quantities

C_R	Reflectivity	[−]
e	Eccentricity	[−]

\odot	Sun
\oplus	Earth
arr	Arrival
calc	Calculated
co	Cut-Off

Physical Quantities

λ	Longitude	[deg]
μ	Gravitational parameter	[km ³ /s ²]
Ω	RAAN	[deg]
ω	Argument of periapsis	[deg]
ω_{\oplus}	Earth's angular rate	[rad/s]
Φ	Latitude	[deg]
θ	True anomaly	[deg]
A	Area	[m ²]
a	Semi-major axis	[km]
f	Frequency	[Hz]
i	Inclination	[deg]
M	Mean anomaly	[deg]
m	Mass	[kg]
p	Pressure	[N/m ²]
R	Heliocentric distance	[km]
r	Relative distance	[km]
T	Orbital period	[s]
V	Heliocentric velocity	[km/s]
v	Relative velocity	[km/s]

dep	Departure
filt	Filtered
pert	Perturbing
rot	Rotation
syn	Synodic
tot	Total

Acronyms

AU	Astronomical Unit
DoF	Degree of Freedom
ECI	Earth-Centered Inertial
FFT	Fast Fourier Transform
FPS	Frames Per Second
GA	Genetic Algorithm
IFFT	Inverse Fast Fourier Transform
LPF	Low Pass Filter
ODE	Ordinary Differential Equation
PGA	Powered Gravity Assist
RAAN	Right Ascension of the Ascending Node
S/C	SpaceCraft
SoI	Sphere of Influence
SRP	Solar Radiation Pressure
ToF	Time of Flight

Subscripts/Superscripts

$_{\text{J}}$	Jupiter
$_{\text{M}}$	Mars
$_{\text{N}}$	Neptune

Interplanetary Explorer Mission

The PoliMi Space Agency is carrying out a feasibility study for an *Interplanetary Explorer Mission* visiting three different planets in the Solar System: Neptune, Jupiter and Mars.

This first part of the report aims at performing a preliminary mission analysis, which consists in the study of the transfer options from the departure planet (Neptune) to the arrival planet (Mars), with a powered gravity assist flyby at Jupiter. The interplanetary trajectory will be primarily selected based on the minimization of the overall mission cost (measured through the total ΔV).

Because of the lack of assigned constraints, the final solution will be chosen by considering a tradeoff among ΔV_{tot} , Δt_{tot} , t_{dep} .

1.1 Design Process

The design of the interplanetary trajectory will be based on the *patched-conics* method, thus resulting in two Lambert's arcs: Neptune \rightarrow Jupiter and Jupiter \rightarrow Mars, matched with a flyby of Jupiter. Planetary departure and orbit insertion is not taken into account throughout this analysis: initial and final state vectors are assumed equal to those of the respective planets.

The design process may then translate into a constrained parametric optimization problem with 3DoFs: t_{dep} , ToF₁, ToF₂. For computing its solution there are, basically, two available approaches:

- grid search throughout a 3D array⁽¹⁾
- advanced optimization algorithms (e.g. genetic algorithm, particle swarm optimization, etc.)

It has been chosen to seek for the optimal solution, over an extremely wide domain, by means of genetic algorithms and then validate such results by means of a restricted grid search.

1.1.1 Design Constraints

During the designing process the most important considerations regard a proper selection of the time windows and in general the overall timing of the mission. The range of departure dates here analyzed corresponds to one orbital period of Neptune (~ 165 years), starting on January 1st, 2019. The choice of the ToF windows is based on the synodic periods, which may be seen as the simplest measure of the repetition frequency

⁽¹⁾each of its element is associated with a different interplanetary trajectory

of a two-planet relative configuration.⁽²⁾

$$T_{\text{syn}} = \frac{T_1 \cdot T_2}{|T_1 - T_2|} = \begin{cases} \text{Neptune-Jupiter } (\mathfrak{N} \leftrightarrow \mathfrak{J}) : & 12.785 \text{ years} \\ \text{Jupiter-Mars } (\mathfrak{J} \leftrightarrow \mathfrak{M}) : & 2.235 \text{ years} \end{cases} \quad (1.1)$$

We will hence set the maximum allowed ToF as a certain multiple of T_{syn} . Specifically, as we will later explain in Subsec. 1.1.3: $\text{ToF}_1^{\max} = 1.3T_{\text{syn}}^{\mathfrak{N}\mathfrak{J}}$, $\text{ToF}_2^{\max} = 3T_{\text{syn}}^{\mathfrak{J}\mathfrak{M}}$.

A further restriction on the departure window has been made in order to guarantee a reasonable waiting time for obtaining valuable scientific results from the mission. The maximum allowed departure date is set on January 1st, 2050.

One more constraint has to be introduced with regard to the minimum altitude⁽³⁾ during the flyby of Jupiter. As reported in [Lam08] the closest ever approach of Jupiter was performed by the *Juno* spacecraft at 4500 km, hence a lower bound of 2000 km may be reasonably assumed.

1.1.2 Grid Search Setup

In order to obtain some useful results for the validation of other algorithms a brute-force iterative procedure has been implemented. The use of three loop cycles allowed the creation of a 3D array containing the ΔV for all the plausible missions that could be performed inside the selected launch window.

The core of the algorithm can be summarized by the following pseudo-code:

Algorithm 1 Calculate ΔV Entries

```

for each possible departure date do
    for each possible  $\text{ToF}_1$  do
        Get planets positions
        Compute first Lambert's arc (Neptune  $\rightarrow$  Jupiter)
        for each possible  $\text{ToF}_2$  do
            Get planets positions
            Compute second Lambert's arc (Jupiter  $\rightarrow$  Mars)
            Compute PGA burn at Jupiter as a function of heliocentric incoming (1st Lambert)
            and outgoing (2nd Lambert) velocities.
            if No constraint violation then
                Compute total cost and fill the corresponding entry in the 3D array
            end if
        end for
    end for
end for
Search for the smallest value of  $\Delta V_{\text{tot}}$  inside the array

```

This procedure allows to obtain an estimation of the most efficient set of trajectories among the three planets. Its precision is directly correlated to the choice of the time

⁽²⁾such a definition is actually based on assuming circular planetary orbits, but given the close-to-zero eccentricity of the planets involved, the choice here made proves quite accurate

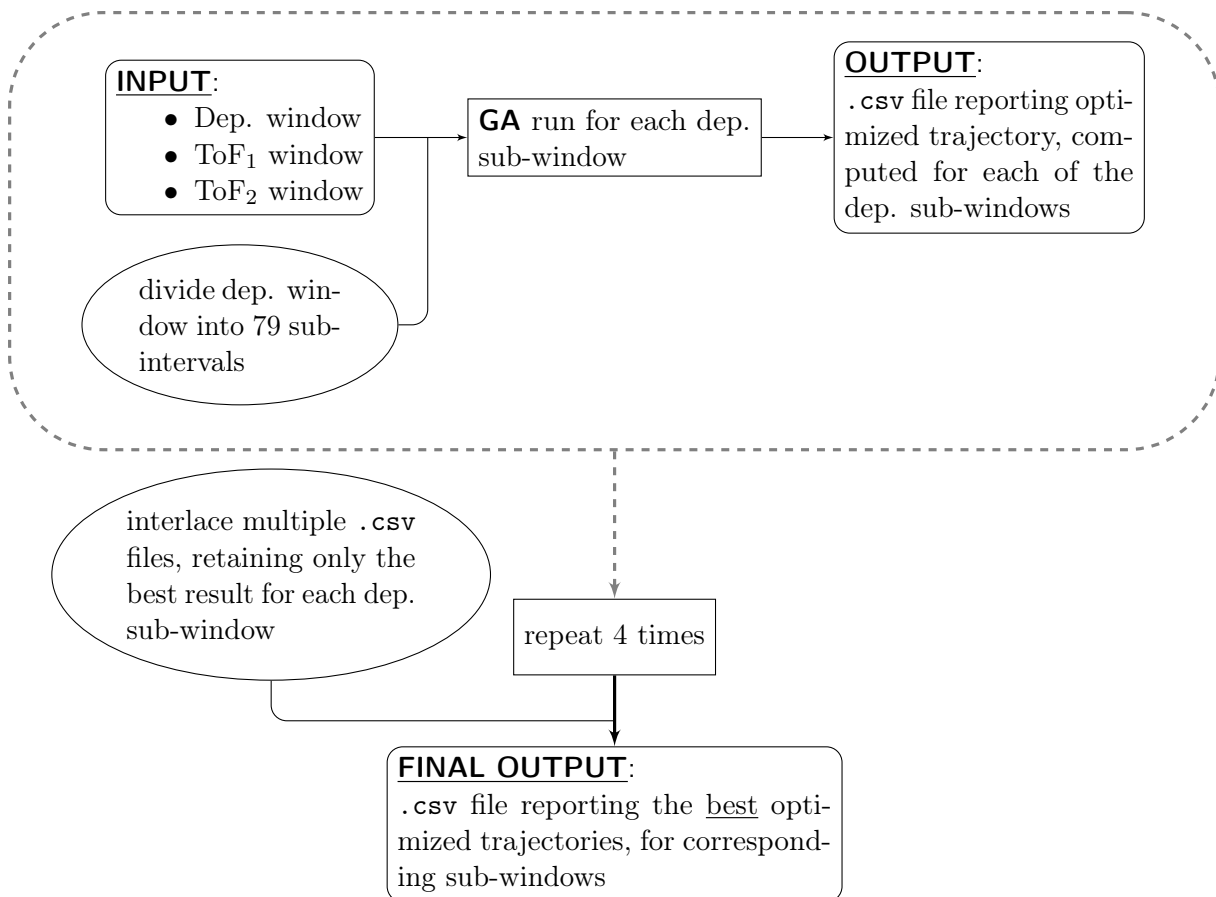
⁽³⁾the S/C has to be kept above the cloud tops of Jupiter to avoid any atmospheric effects

intervals: as the number decreases the result of the algorithm is going to converge to the absolute minimum. However this has the effect of increasing significantly the computational time, hence a trade-off has to be achieved. It was decided to prioritize the increase in discretization of the second time of flight rather than the first one. The cruise from Jupiter to Mars is in fact associated with planets which undergo larger differences in position over time due to the much smaller revolution periods with respect to Neptune. It was found that selecting an interval $\Delta t_{\text{ToF}_1} = 60$ days, $\Delta t_{\text{ToF}_2} = 10$ days and allowing for parallel computation in different CPUs the algorithm offered the best achievable balance between precision and reasonable times of computation.

1.1.3 Genetic Algorithm Setup

Genetic algorithms are likely to converge to the global minimum of the inputted cost function, rather than some local optima. Nevertheless, this is never guaranteed,⁽⁴⁾ especially whenever the cost function is highly nonlinear and subject to strong variations over a wide domain.

The chosen strategy is indeed aimed at obtaining the most accurate and optimized results, yet accounting for reasonable time constraints.



In tuning the input windows for ToF_1 and ToF_2 , it can be immediately noticed that the more we extended either window, the lower is the cost of the related burn in correspondence

⁽⁴⁾each run may in general converge to different results, due to the random initialization of the algorithm

of the optimal trajectory, which eventually tends to a certain asymptotic value as we further extend the time windows.⁽⁵⁾ Hence, if we were to allow for arbitrarily large ToFs, the GA would then converge to ΔV values in the order of those found in Appendix, which nevertheless determines an inadmissible overall mission time, requiring to set proper constraints.

Being the mission from an outer to inner planet, the orbital velocity will be much higher at the end of the mission, which in turn determines a final burn that is likely to be the highest. This is indeed providing a hint on how to select proper weighting coefficients, whose meaning is “which of the two Lambert’s arcs shall be taken as an optimization-priority?”.⁽⁶⁾ As a final choice, after a few iterating attempts, the following input windows were selected:

$$\text{ToF}_1^{\max} = 1.3T_{\text{syn}}^{\Psi^4} = 16.621 \text{ years} \quad \text{ToF}_2^{\max} = 3T_{\text{syn}}^{\Psi^4\sigma} = 4.422 \text{ years}$$

whose output, as obtained from multiple interlaced GA runs, can be found in Appendix.

In addition, such decision turns out to be consistent with a comparable mission: *Voyager II*, for which it took 12 years to reach Neptune, taking advantage of three gravity assists.

1.1.4 Selection of a Final Solution

At the outset, it was chosen to compute an estimate of the asymptotic value⁽⁷⁾ we may obtain, if we were to allow for arbitrarily large ToFs, by setting as constraints: $\{\Delta t_0^{\max} = T_{\Psi}; \quad \text{ToF}_1^{\max} = 4T_{\text{syn}}^{\Psi^4}; \quad \text{ToF}_2^{\max} = 4T_{\text{syn}}^{\Psi^4\sigma}\}$.

The lowest cost is achieved in correspondence of:

Departure	Flyby	Arrival	ΔV [km/s]
2027 Jan 27 at 10:44:34	2064 May 10 at 19:42:21	2067 Oct 22 at 09:56:04	8.11164

which is nevertheless inadmissible, due to the excessive transfer time (~ 40 years).

As already stated in (Subsec. 1.1.3), setting instead $\{\Delta t_0^{\max} = T_{\Psi}; \quad \text{ToF}_1^{\max} = 1.3T_{\text{syn}}^{\Psi^4}; \quad \text{ToF}_2^{\max} = 3T_{\text{syn}}^{\Psi^4\sigma}\}$ yields as optimum:

Departure	Flyby	Arrival	ΔV [km/s]
2033 May 29 at 23:23:04	2050 Jan 11 at 15:21:04	2054 May 15 at 14:35:30	12.16010
$\text{ToF}_1 = 6070.665 \text{ days} \quad \text{ToF}_2 = 1584.968 \text{ days}$			

⁽⁵⁾in other words, setting a wider time window corresponds to accounting for an increased number of planetary relative configurations, among which a better one is likely to be found

⁽⁶⁾the answer is of course: the second one, whose related weighting coefficient will be higher

⁽⁷⁾i.e. as low as possible

which the team has eventually selected as the final compromise-solution.

In order to corroborate the validity of our design choices, the **porkchop plot** might be selected as a first validation tool.

It can be experienced that the burn in correspondence of the PGA tends to be much smaller in magnitude than the two other burns. As a consequence we may reasonably plot the two diagrams by separately considering each arc, just as if they were uncoupled problems, hence temporarily neglecting the value of the burn performed at the flyby planet.

Within the following plots the chosen trajectory is highlighted by a marker.

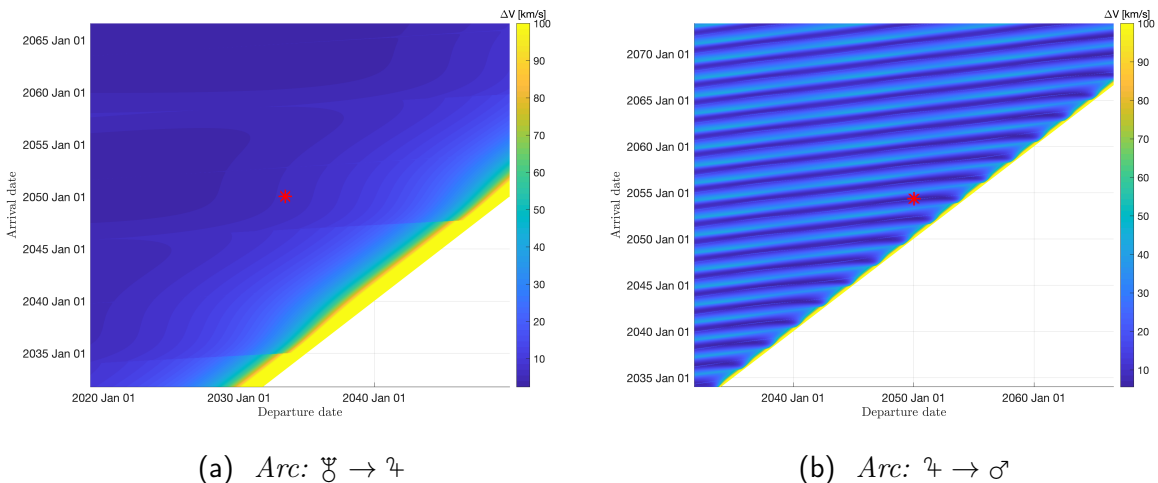


Figure 1.1: *Porkchop plots (neglecting the PGA burn)*

As expected, it can be observed that the selected trajectory lies a little off from the global optima of Figs. 1.1a, 1.1b, since the optimization of one single trajectory may in general correspond to poor results for the other.

1.2 Results and Conclusions

1.2.1 Heliocentric Trajectories

The two heliocentric transfer orbits associated with the selected solution, computed through the Lambert solver, can be characterized using the Keplerian elements seen in Tab. 1.1:

Table 1.1: *Heliocentric transfer orbits*

Departure	Arrival	a [AU]	e [-]	i [deg]	Ω [deg]	ω [deg]	$[\theta_{\text{dep}}, \theta_{\text{arr}}]$ [deg]
$\text{☿} \rightarrow \text{♀}$	2033 May 29	2050 Jan 11	38.89	0.8812	1.60	104.43	56.41 [216.41, 318.00]
$\text{♀} \rightarrow \text{♂}$	2050 Jan 11	2054 May 15	3.52	0.6061	4.20	113.39	203.62 [-198.16, 2.53]

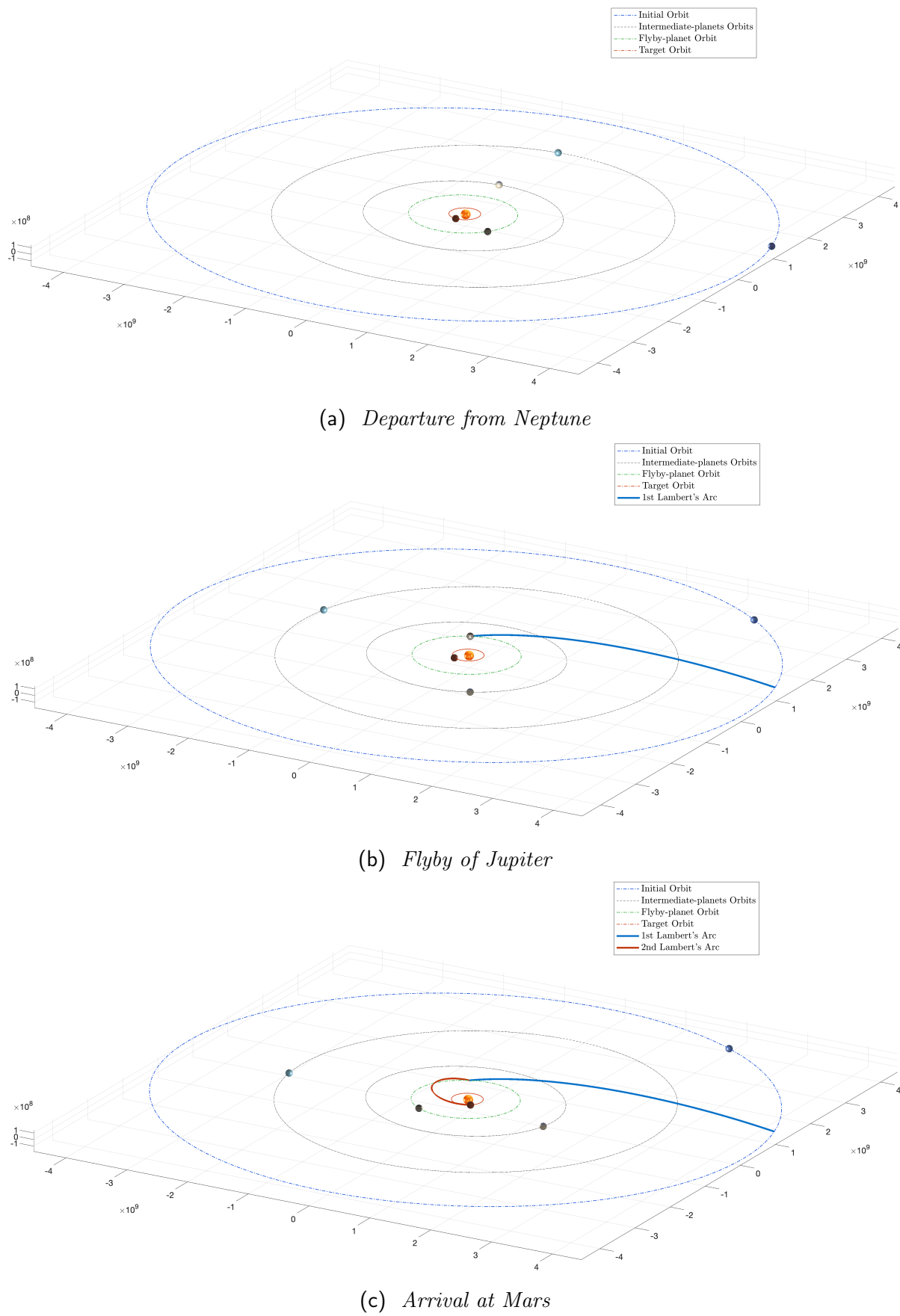


Figure 1.2: *Heliocentric configurations*

1.2.2 Powered Gravity Assist

Using the incoming and outgoing heliocentric velocities of the S/C it was possible to completely characterize the flyby hyperbola in a Jupiter-centered perifocal frame. Since $\underline{\mathbf{v}}_{\infty}^-$ and $\underline{\mathbf{v}}_{\infty}^+$ will in general differ from each other, the flyby is required to be powered: an impulsive burn $\Delta V_{\text{PGA}} = 0.233725 \text{ km/s}$ is provided at the common perigee of the two hyperbolic arcs. The results that were obtained are displayed in Tab. 1.2 and a plot of the orbit is shown in Fig. 1.3.

Table 1.2: Incoming and outgoing hyperbolic trajectories, inside SoI₄

r_p [km]	h_p [km]	e^- [-]	e^+ [-]	v_{∞}^- [km/s]	v_{∞}^+ [km/s]	$\Delta V = \ \underline{\mathbf{V}}^+ - \underline{\mathbf{V}}^-\ $ [km/s]	Δt_{SoI} [days]
73876.634	3965.634	1.03362	1.01756	7.59399	5.48779	12.77224	147.37 days

The permanence time inside the SoI has been computed using the hyperbolic time law and considering the intersection between the two arcs and a sphere, where the boundary of the latter is defined by the condition:

$$r_{\text{SoI}}^{\frac{7}{4}} \leq R_{\odot \frac{7}{4}} \left(\frac{m_{\frac{7}{4}}}{m_{\odot}} \right)^{\frac{2}{5}} = 48\,652\,651 \text{ km}$$

It can be noted that the considerable decrease in heliocentric velocity ΔV , achieved after the flyby, will mainly affect the V_y component:

$$\underline{\mathbf{V}}^- = \begin{Bmatrix} -11.7668403164062 \\ -13.2841477532301 \\ 0.411952768117762 \end{Bmatrix} \frac{\text{km}}{\text{s}} \quad \underline{\mathbf{V}}^+ = \begin{Bmatrix} -9.21171471407473 \\ -0.772235992445798 \\ 0.643264211137162 \end{Bmatrix} \frac{\text{km}}{\text{s}}$$

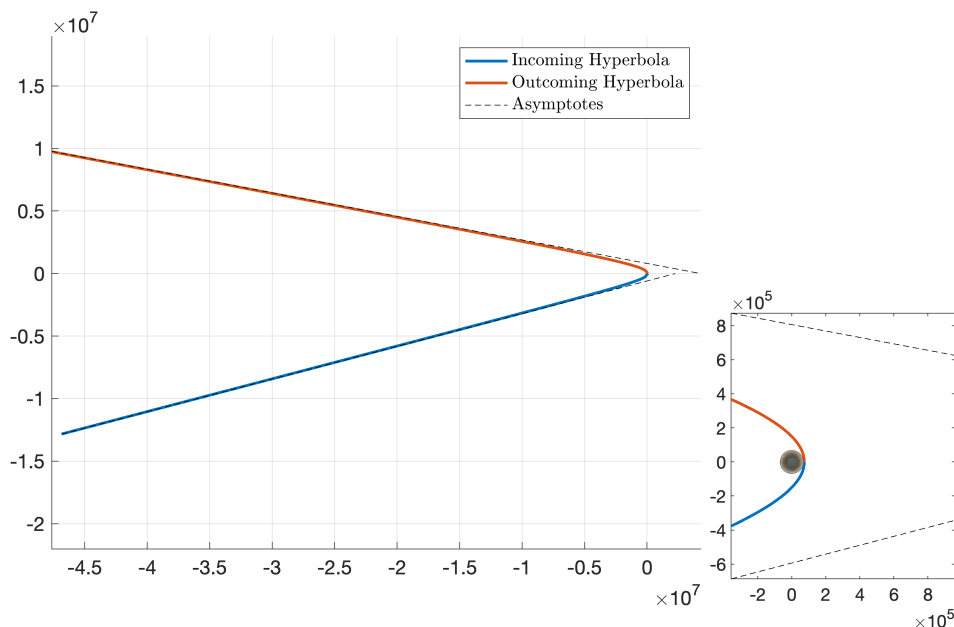


Figure 1.3: Flyby detail

1.2.3 Total Mission Cost

The cost of the mission is here detailed in Tab. 1.3:

Table 1.3: *Mission cost*

	ΔV_{dep}	ΔV_{PGA}	ΔV_{arr}	ΔV_{tot}
Cost of the burn [km/s]	5.837899	0.233725	6.088478	12.160102

It can be seen that, as it was anticipated earlier, the ΔV associated with the powered flyby is much smaller than those associated with departure and final orbit insertion. Moreover, these last two burns have turned out to be almost equal in magnitude, reaching a value of about 6 km/s.

Besides these results supposedly being the best trade-off in terms of propellant cost and time of flight, they probably would not be feasible for a real-life mission: the overall ΔV is still too high for a state of the art upper-stage to achieve. This is particularly true when considering a realistic scenario of a very limited propellant budget for a spacecraft at Neptune but even if the launch of a spacecraft from Neptune were supported by the same facilities and resources available here on Earth, the proposed trajectory would result unsuitable anyway.

During the analysis two main possible solutions to the problem have been identified:

- *Increase total ToF.* As already stated (Subsec. 1.1.3), whenever the overall time of the mission is increased the total optimal cost of the mission drops asymptotically to a magnitude around 8 km/s. This indeed would be a value that the state of the art engines could reach, at least in the discussed hypothesis. The incredibly long duration of the mission (~ 40 years) makes it however unsuitable for any scientifically significative mission.
- *Increase the number of Flybys.* For this mission analysis it was required to perform only one gravity assists during the cruise from Jupiter to Mars. In a real-life mission a larger number of gravity assists could be performed in order to exploit their ability to increase the heliocentric speed of the S/C. This would reduce the overall cost of the mission, making the transfer between the two planets at least plausible with the current technologies. This consideration is indeed supported by actual past missions data: *Voyager II* performed 3 flybys before reaching Neptune, with technologies already available over 40 years ago.

Planetary Explorer Mission

The PoliMi Space Agency wants to launch a Planetary Explorer Mission, to perform Earth observation.

This part of the report aims at studying the effect of orbit perturbations on a HEO orbit. Specifically, the J_2 effect and SRP will be taken into account: different propagation methods are implemented and compared, while frequency analysis is employed to highlight the main harmonics associated with the perturbing effects.

The analysis will also dwell on ground track estimation and an orbit modification to achieve a repeating ground track will be proposed.

2.1 Initial Orbit Characterization

The initial Earth-centered orbit is characterized by the following orbital elements at epoch:

Table 2.1: *Initial orbital elements*

a	e	i	Ω	ω	θ
29437 km	0.451	83.0581°	35°	27°	30°

The perturbations here accounted for are:

- J_2 effect (i.e. first zonal harmonic), due to Earth's oblateness:

$$\underline{\mathbf{a}}_{J_2} = \frac{3}{2} \frac{J_2 \mu R_\oplus^2}{r^5} \left[\left(5 \frac{z^2}{r^2} - 1 \right) x\hat{\mathbf{i}} + \left(5 \frac{z^2}{r^2} - 1 \right) y\hat{\mathbf{j}} + \left(5 \frac{z^2}{r^2} - 3 \right) z\hat{\mathbf{k}} \right] \quad (2.1)$$

(where $J_2 = 0.00108263$)

- Solar Radiation Pressure (SRP):

$$\underline{\mathbf{a}}_{\text{SRP}} = (\text{switch}) \cdot p_{\text{SR@1AU}} \left(\frac{AU}{r_{\odot \rightarrow S/C}} \right)^2 C_R \frac{A}{m} \hat{\mathbf{r}}_{\odot \rightarrow S/C}$$

where **switch** is a boolean parameter that identifies whether or not the S/C is in eclipse, by means of an algorithm proposed in [Val01].

For SRP an area-to-mass ratio $A/m = 0.5 \text{ m}^2/\text{kg}$ will be assumed, along with a reflectivity $C_R = 1$.

2.2 Ground Track

During the flight of a S/C on its trajectory, the ground track will be subject to a westward shift. This is due to two main effects.

- *Earth rotation*
- J_2 perturbation, which has a secular effect on the RAAN

$$\Delta\Omega_{\text{tot}} = \underbrace{\left[-\frac{2\pi T_{\oplus}}{T} \right]}_{\Delta\Omega_{\text{rot}}} + \underbrace{\left[-\frac{3\pi J_2 R_{\oplus}^2 \cos i}{(1-e^2)^2 a^2} \right]}_{\Delta\Omega_{J_2}} \quad \left(\text{recalling: } T = 2\pi\sqrt{\frac{a^3}{\mu}} \right) \quad (2.2)$$

$\Delta\Omega_{\text{rot}}$	$\Delta\Omega_{J_2}$	$\Delta\Omega_{\text{tot}}$
-210.0039°	-0.0052°	-210.0092°

It can be immediately seen that the effect of the J_2 perturbation is incredibly smaller than that due to Earth's rotation. The reason lies in the nature of the orbit: it is almost polar ($i \sim 90^\circ$) and has high value of a , therefore $\Delta\Omega_{J_2} \sim 0$. This will result in extremely similar outcomes on the ground tracks with and without J_2 . In Figs. 2.1, 2.2, 2.3 the comparison between the two different propagations has been reported.

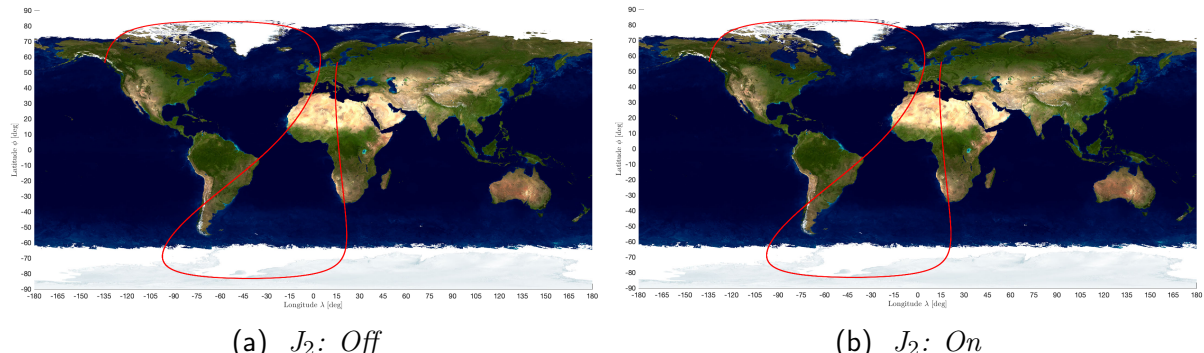


Figure 2.1: *Ground track after 1 orbit*

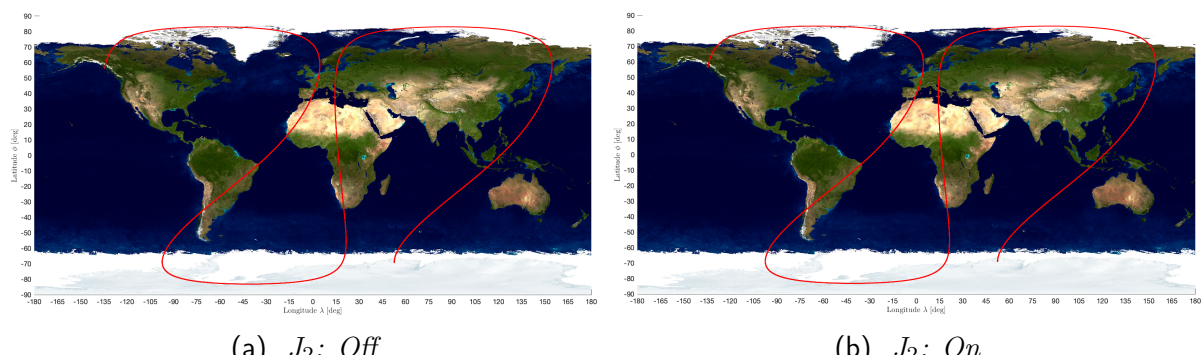


Figure 2.2: *Ground track after 1 day*

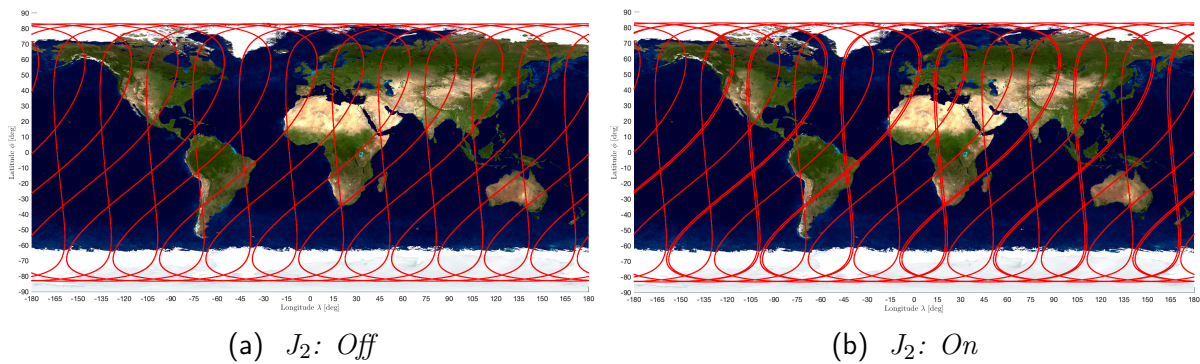


Figure 2.3: *Ground track after 10 days*

2.2.1 Ground Track Repetition

In order for the ground track to repeat itself over time, the following condition has to be enforced:

$$m2\pi = n\Delta\Omega_{\text{tot}} \quad (2.3)$$

where n is the number of orbital periods and m is the number of sidereal days before the repetition. The repetition is exact only if these two numbers are integers ($n, m \in \mathbb{N}$).

During the preliminary analysis it was seen that considering the effect of J_2 after $n = 12$ orbits and $m = 7$ days, the ground track is almost repeated. This is true even for the unperturbed case (with even higher precision).

An iterative procedure which obtains the values of n and m for a specific orbit was implemented to validate the results. First of all, an estimation of m has been obtained using Eq. 2.3, evaluating the expression using different values of n . This provided some information about the number of days elapsed after n orbits (such a value will be in general non-integer).

$$m_{\text{calc}} = \text{func}(n, \Delta\Omega_{\text{tot}}) = \frac{n}{2\pi} \Delta\Omega_{\text{tot}} \quad (2.4)$$

The set $\{m, n\}$ was selected as the values such that the difference between m_{calc} and its closer integer is smaller than a given tolerance (i.e. $m_{\text{calc}} - \text{round}(m_{\text{calc}}) < \text{tol}$). By trial and error it was decided to set $\text{tol} = 10^{-3}$ which yields: $n = 12$, $m = 7$ for both cases (J_2 on/off). This means that the ground track of the orbit is very close to repeating itself for the outputted condition, as it can be seen in Fig. 2.4.

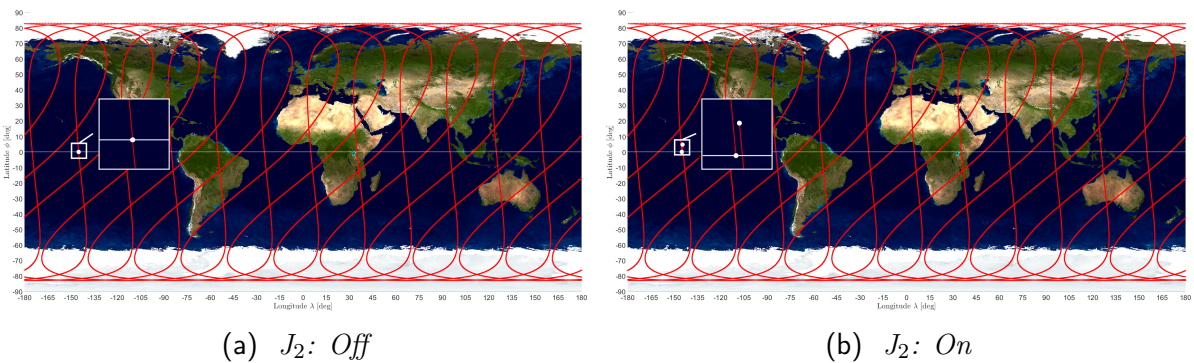


Figure 2.4: Ground track of the orbit after $n = 12$ orbits, $m = 7$ days

In order to obtain an exact repetition of the ground track a modification has been proposed. It was required to modify the original orbit as little as possible and only in terms of its semi-major axis. Plugging Eq. 2.2 into Eq. 2.3 and solving for a yields:

Table 2.2: *Proposal for modified semi-major axis*

Original orbit	Modified orbit (J_2 : Off)	Modified orbit (J_2 : On)
a [km]	29437	29436.63

It can be immediately noticed that the modification would be quite small compared to the initial orbit, in the order of hundreds of meters. This means that the initial orbit already offered a good solution for the achievement of repeated passages over a ground station. On top of that, even with a modified semi-major axis, the ground track does not repeat exactly anyway when accounting for the J_2 effect, as it can be seen in Fig. 2.5.

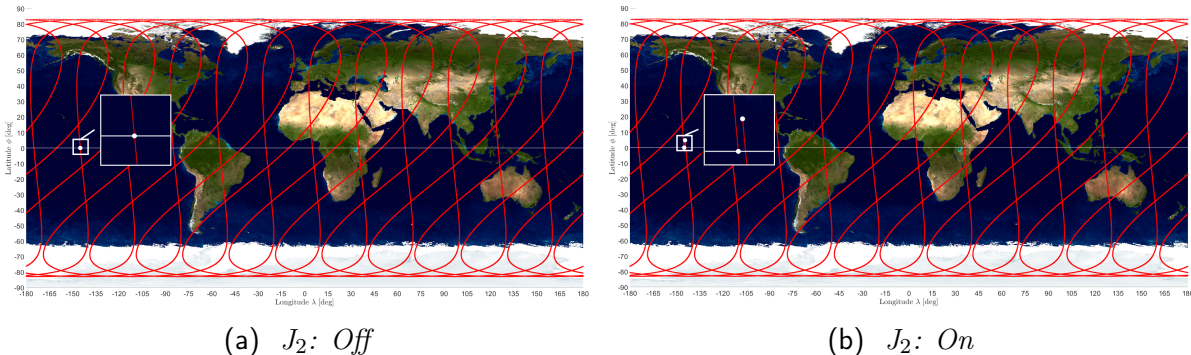


Figure 2.5: *Ground track of the modified orbit after $n = 12$ orbits, $m = 7$ days*

The reason was found to be inherently associated with the nature of the perturbed two body problem. The formula used to determine the repetition of the ground track (Eq. 2.3) is indeed an approximation, a complete expression to impose the repetition condition can be found in [Vti12]:

$$\tau := \frac{m}{n} = \frac{\omega_{\oplus} - \dot{\Omega}}{\dot{M} + \dot{\omega}} \quad (2.5)$$

The gravitational perturbation due to J_2 determines secular effects not only in terms of nodal regression ($\dot{\Omega} \neq 0$) but also changes the argument of perigee ($\dot{\omega} \neq 0$) and the mean anomaly ($\dot{M} \neq 0$). The results obtained with Eq. 2.3 are imposing no actual repetition of the ground track.

2.3 Orbit Propagation

For propagating the initial orbit and hence determine the corresponding time-evolution of the orbital elements, two different approaches will be implemented and compared.

- Cartesian coordinates propagation:

$$\text{solve } \ddot{\mathbf{r}} = -\frac{\mu}{r^3} \mathbf{r} + \underline{\mathbf{a}}_{\text{pert}} \xrightarrow{\text{car2kep}} \underbrace{\{a, e, i, \Omega, \omega, \theta\}}_{:=\underline{\alpha}(t)} \quad \forall t$$

- Gauss planetary eqs.:

$$\text{solve } \begin{cases} \dot{a} &= (\dots) \\ \dot{e} &= (\dots) \\ \vdots & \\ \dot{\theta} &= (\dots) \end{cases} \xrightarrow{\text{tnh}} \underline{\alpha}(t) \quad \forall t$$

$$\underline{\mathbf{a}}_{\text{pert}}^{(\text{tnh})} = [\hat{\mathbf{t}} | \hat{\mathbf{n}} | \hat{\mathbf{h}}]^\top \underline{\mathbf{a}}_{\text{pert}}^{(\text{cart})}$$

It can be experienced that, for a given tolerance assigned to the ODE solver, there is no difference in terms of **accuracy** between the two methods. This may for instance be proved by computing the error in the infinity-norm, relative to the time evolutions obtained for each element. Propagating the initial conditions (Tab. 2.1) for 100 orbits and setting **Relative Tolerance** = 10^{-13} , **Absolute Tolerance** = 10^{-14} yields for instance:

Table 2.3: *Infinity-norm error between cartesian and gaussian propagation*

	a	e	i	Ω	ω	θ
$\ \mathbf{err}\ _\infty$	3.04E-06 km	5.73E-11	6.84E-11°	1.20E-10°	2.97E-09°	3.79E-06°

Such values are relatively close to round-off errors, which indeed confirms our initial statement.

A substantial difference may instead be highlighted in terms of computational **efficiency**, as shown in Fig. 2.6: for the range of discretization levels covered in this plot, Gauss planetary eqs. are about twice as quick as cartesian coordinates integration.

For the above mentioned reasons, it is then clear the superiority of Gauss eqs. which will henceforth be used to propagate the orbit, for the remainder of our analyses. Setting 2019, March 21, 12:00 as our epoch, yields the following time evolution, after 500 orbits:

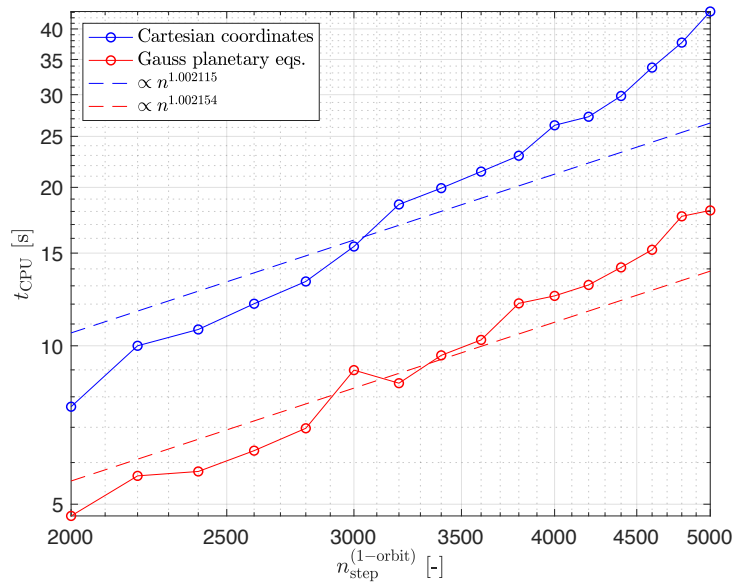


Figure 2.6: *Computational cost dependence upon the number of time steps for each orbit*

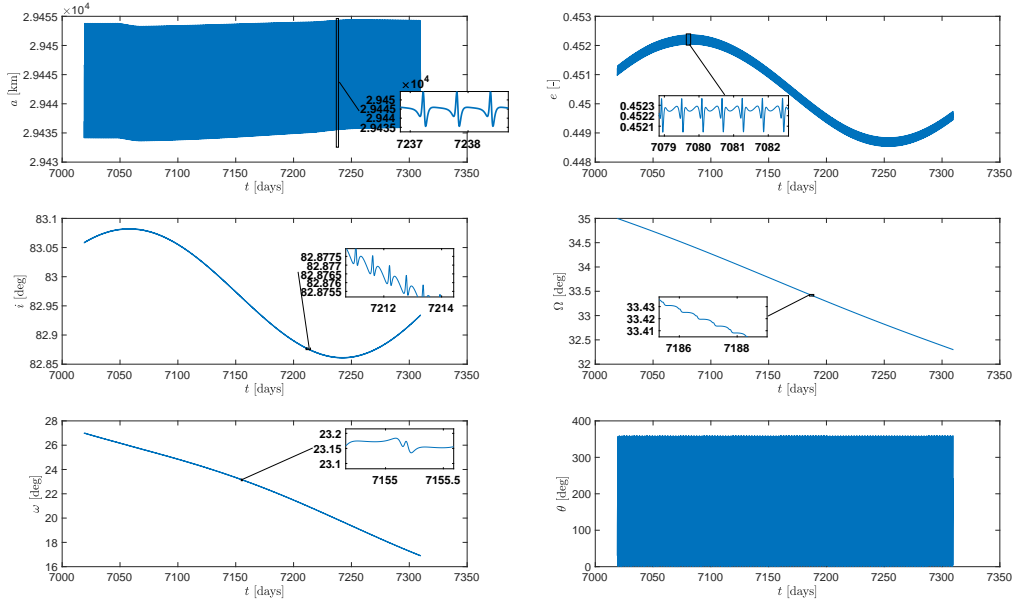


Figure 2.7: Orbit propagation ($J_2 \& SRP$), after 500 revolutions

Besides the short-period oscillations which are affecting each orbital element, it is immediate to recognize:

- secular variation of Ω, ω due to J_2 effect⁽¹⁾
- long term oscillation of e, i due to SRP
- short term oscillation of all orbital elements

We may at this point further extend the integration timespan, in order to observe how the orbit's shape and orientation would change throughout the S/C lifecycle, provided that no orbit maintenance maneuver is performed. Propagating the initial assigned orbital elements for 10000 orbits (~ 14.44 years) yields:

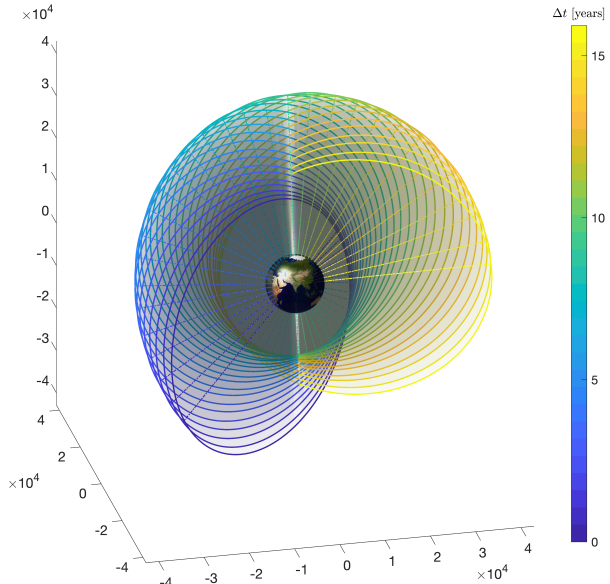


Figure 2.8: Orbit evolution after 10000 revolutions

⁽¹⁾ $i \in (63.4^\circ, 90^\circ) \rightarrow \begin{cases} \text{nodal regression} & (\dot{\Omega} < 0) \\ \text{perigee regression} & (\dot{\omega} < 0) \end{cases}$

2.4 Spectral Frequency Analysis

As it can be observed in Fig. 2.7, a raw numerical propagation produces a time evolution of the orbital elements characterized by several high frequency oscillations. In order to obtain a more meaningful representation, frequency analysis can be a useful tool. Computing the Fast Fourier Transform⁽²⁾ (FFT) of the signal identified by each element's time evolution⁽³⁾ highlights the presence of negligible (i.e. small amplitude) high frequency harmonics. It is then natural to filter out the evolution accordingly, thus building what essentially becomes a low-pass filter.

A detailed examination of the spectra, along with a trial-and-error strategy, has led to the following choice of cut-off frequencies:

$$\underline{f}_{\text{co}} = 10^{-6} \cdot \begin{bmatrix} 1 & 1 & 1 & 5 & 5 \\ \downarrow & \downarrow & \downarrow & \downarrow & \downarrow \\ a & e & i & \Omega & \omega \end{bmatrix} \text{ Hz}$$

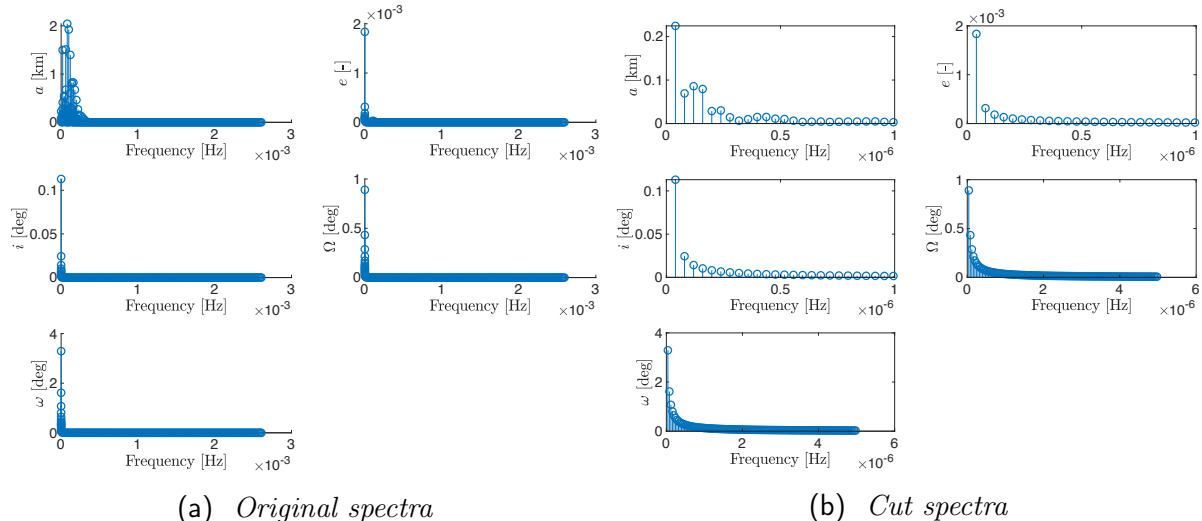


Figure 2.9: Orbital elements spectrum (J_2 & SRP)

We may at this point choose between two different strategies.

1. FFT-based-filtering

time evolution: $\underline{\alpha}(t) \xrightarrow{\text{FFT}}$ frequency spectra $\xrightarrow{\text{LPF}}$ cut spectra $\xrightarrow{\text{IFFT}}$ $\underline{\alpha}_{\text{filt}}(t)$

2. Moving-average-filtering

The underlying idea behind this operator is that of having a sort of sliding window with fixed size⁽⁴⁾ that scrolls through the original evolution and replaces each value with the local mean. The size of the window must then be chosen consistently with the previously established cut-off frequencies. The answer lies in Nyquist-Shannon **sampling theorem**, which states: “*The minimum sampling frequency of a signal such that it will not distort its underlying information, has to be double the frequency*

⁽²⁾which, as we recall, allows us to move from the time-domain to the frequency-domain

⁽³⁾each amplitude is specifically identified by the real part of the FFT

⁽⁴⁾specified in terms of number of adjacent discrete points

of its highest frequency harmonic”.

In our contest, this translates into setting a sliding window with a size that is at most half⁽⁵⁾ the one associated with the cut-off frequency, namely:

$$N^{(k)} = \text{floor}\left(\frac{1}{2} \frac{f_s}{f_{co}^{(k)}}\right)$$

where f_s is the sampling frequency, relative to the time step-size of the original (unfiltered) propagation. In addition, it can be experienced that the best results are obtained selecting a centered moving-average.

The outcomes of adopting either strategy are reported in Fig. 2.10, where the original signal is the same as in Fig. 2.7.

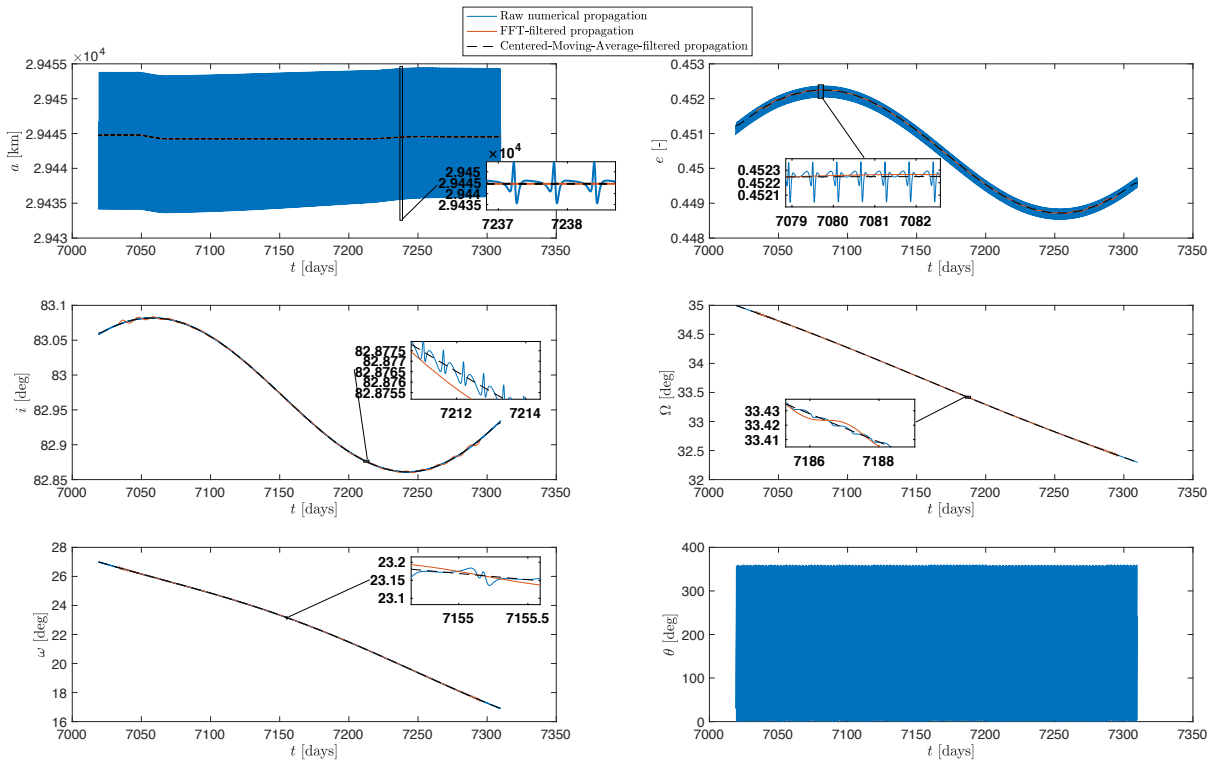


Figure 2.10: Comparison between filtered and unfiltered orbital elements propagation

There are several situations in which being provided with a filtered propagation proves quite meaningful. For instance, among the deliverables produced by the team, a movie showing the orbit’s evolution over time can be found.

The movie has been rendered with a framerate of 24 FPS (i.e. 0.04167 Hz), right from the filtered propagation. It was indeed noticed that the raw numerical propagation was instead subject to undersampling, hence resulting in an animation affected by aliasing phenomena.

⁽⁵⁾the smaller, the less we filter (i.e. closer to original)

2.5 Comparison with Real Data

In order to validate the numerical propagation, a comparison with the results produced by the NASA HORIZONS propagator ([HOR]) has been made for the *NAVSTAR68* satellite. The latter is an American navigation satellite, operating from a semi-synchronous MEO, at an altitude of 20459 km and an inclination of 55° in slot 5 of plane C of the GPS constellation. The orbital elements evolution obtained by HORIZONS has been downloaded as a .csv file and plotted against the results obtained propagating the same initial condition with our model.

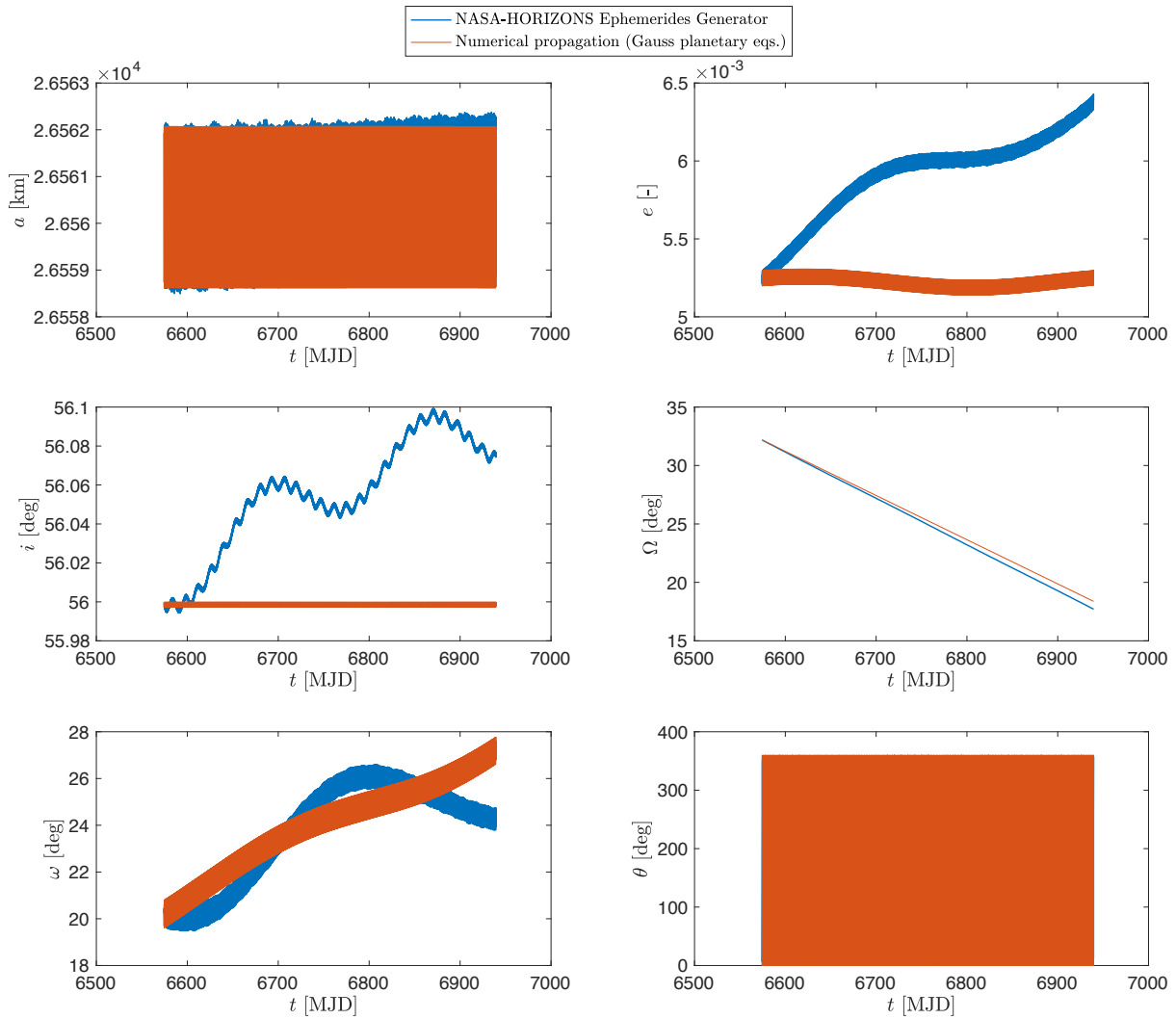


Figure 2.11: Comparison between NASA HORIZONS and numerical propagation (J_2 & SRP)

- An excellent match is achieved in terms of a and Ω
- Acceptably good results can still be observed for ω
- Considerable differences may instead be highlighted for the evolution of e and i

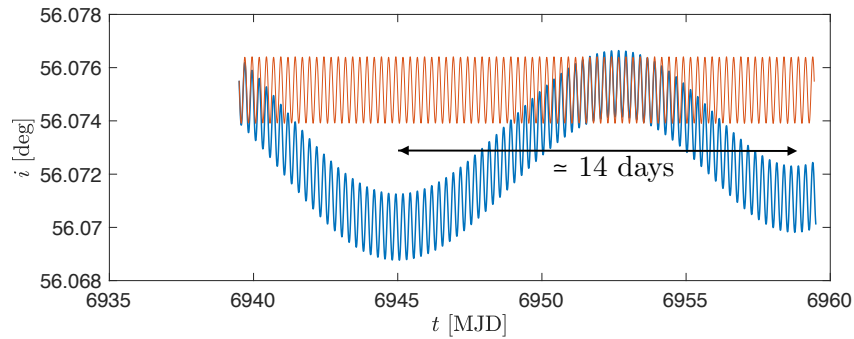


Figure 2.12: *Inclination detail*

From a detailed analysis we may eventually conclude that the difference between the models is basically due to the fact that Moon's third body perturbing effect has been neglected in our own model. Accounting for it would instead translate into considerable long term oscillations. For instance it is immediate to notice an oscillation period of ~ 14 days, namely half the revolution period of the Moon around Earth, which indeed confirms our assumption.

Bibliography

- [Bat99] Richard H Battin. *An Introduction to the Mathematics and Methods of Astrodynamics, revised edition*. American Institute of Aeronautics and Astronautics, 1999.
- [Cur13] Howard D Curtis. *Orbital mechanics for engineering students*. Butterworth-Heinemann, 2013.
- [HOR] Nasa HORIZONS. <https://ssd.jpl.nasa.gov/horizons.cgi>.
- [Lam08] Try Lam, Jennie Johannessen, and Theresa Kowalkowski. “Planetary protection trajectory analysis for the Juno mission”. In: *AIAA/AAS Astrodynamics Specialist Conference and Exhibit*. 2008, p. 7368.
- [Rog03] Paola Rogata et al. “Guess value for interplanetary transfer design through genetic algorithms”. In: *Advances in the Astronautical Sciences* 114 (2003), pp. 613–627.
- [Val01] David A Vallado. *Fundamentals of astrodynamics and applications*. Vol. 12. Springer Science & Business Media, 2001.
- [Vti12] Sharon Vtipil and Brett Newman. “Determining an Earth observation repeat ground track orbit for an optimization methodology”. In: *Journal of Spacecraft and Rockets* 49.1 (2012), pp. 157–164.